Supporting Information for:

Polarized Light Absorption in Wurtzite InP Nanowire Ensembles

M. De Luca,[‡] A. Zilli,[‡,†] H. A. Fonseka,[^] S. Mokkapati,[^] A. Miriametro,[‡] H. H. Tan,[^] L. M. Smith,[^,+] C. Jagadish,[^] M. Capizzi,[‡] and A. Polimeni[‡,]*

[‡]Dipartimento di Fisica and CNISM, Sapienza Università di Roma, Piazzale A. Moro 2, 00185 Roma, Italy

[^]Department of Electronic Materials Engineering, Research School of Physics and Engineering, The Australian National University, Canberra, ACT 0200, Australia

[+]Department of Physics, University of Cincinnati, Cincinnati, Ohio 45221, United States

Corresponding Author

*E-mail address: antonio.polimeni@roma1.infn.it

Present Addresses

†School of Biosciences, Cardiff University, The Sir Martin Evans Building, Museum Avenue, Cardiff CF10 3AX, Wales, United Kingdom

S1. Power and temperature dependence of PL spectra

The attribution of the 1.493 eV peak to the A free exciton (FE) and of the lower energy bands to point (or line) defects stems from the power and temperature studies presented in Figure S1 (a) and (b), respectively.

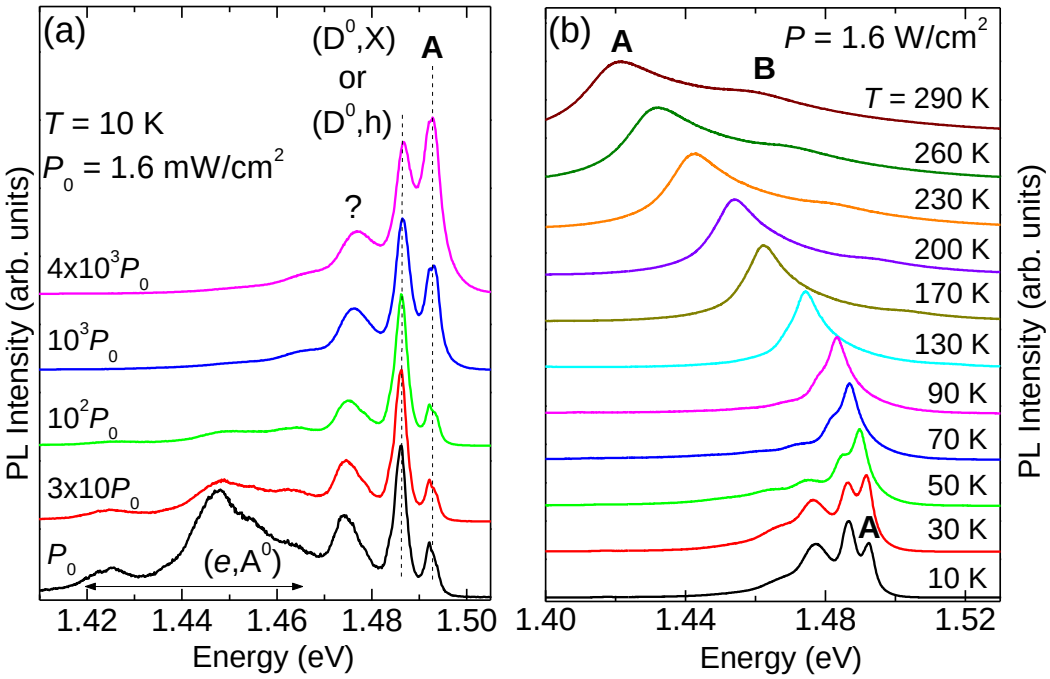

Figure S1. (a) Power dependence of photoluminescence spectra recorded at 10 K on an ensemble of WZ InP NWs. The Γ_7^C-Γ_9^V free exciton recombination is labeled as A. (D^0,X) and (D^0,h) indicate the recombination of an exciton bound to or a hole on a neutral donor D^0, respectively. (e,A^0) indicates free-electron to neutral-acceptor A^0 recombinations. **(b)** Temperature dependence of the PL spectra recorded on the same sample of panel (a). A and B indicate the free-exciton recombination related to the Γ_7^C-Γ_9^V and Γ_7^C-Γ_{7u}^V transitions, respectively.

In the *T*=10 K PL spectra in (a) —recorded for a range of exciting power density spanning ~ 3.5 decades— the peak at 1.493 eV is the highest energy feature and gains in intensity, with respect to the lower energy bands, with increasing excitation power. Therefore, that peak is ascribed to the FE recombination (A) related to the Γ_7^C-Γ_9^V transition. Its energy falls in the energy range of those found in the literature for the band gap transition A in WZ InP. The bands at lower energies are likely due to recombination of excitons or carriers bound to impurities or line defects. The attribution of those bands to spatially indirect type-II transitions is quite unlikely because there is no

significant PL blue-shift with increasing power.[1,2] Furthermore, transmission electron microscopy studies did not show evidence of ZB sections in the NWs.

The 1.42-1.47 eV composite band is labeled as (e,A^0) to indicate various, overlapping free-electron to neutral-acceptor (A^0) recombinations. Specifically, the 1.45 eV peak, ~ 40 meV below the band gap, should be the (e,C^0) recombination in WZ InP (a similar energy difference is observed in the corresponding ZB lattice).[3] The character of the bands at 1.477 eV and 1.487 eV is more puzzling, because they do not saturate sizably at high power. In Ref. 4 a band at 1.486 eV was ascribed to an exciton bound to a neutral donor (D^0,X) and/or to a neutral donor recombination with a free hole (D^0,h).

Some PL spectra recorded at high power density between 10 K and 310 K are displayed in panel (b). When the temperature is raised, deeper states are progressively ionized: The disappearance of all low energy bands at 130 K confirms their extrinsic nature of defect-related states. Above 130 K, the FE recombination progressively turns into a band-to-band recombination. The A band peak exhibits a regular Varshni-like energy shift with temperature, which confirms further its intrinsic nature.[5] From 150 K and up to RT, a shoulder appears about 40 meV above the band-gap emission. It is due to the B resonance related to the Γ_7^C-Γ_{7u}^V transition, as better observed in PLE spectra.

S2. Dependence of PLE spectra and absorption degree of polarization on detection energy.

Figure S2 (a) shows photoluminescence (PL, black line) and PL excitation (PLE, blue and orange lines) spectra taken at 10 K and excited by a laser with polarization vector $\hat{\varepsilon}$ either parallel, $\hat{\varepsilon}_{//}$, or perpendicular, $\hat{\varepsilon}_{\perp}$, to the NW $\hat{c}$ axis. These spectra are labeled $I_{//}$ and $I_{\perp}$, respectively, in the figure. Each couple of polarized PLE spectra was recorded at different detection energies E_{det}, as shown in the Figure and highlighted in the PL spectrum by arrows. A, B, and C indicate the three main transitions of WZ InP NWs. The resulting absorption polarization degrees $\rho_{\mathrm{abs}}(E)=(I_{\perp}-I_{//})/(I_{\perp}+I_{//})$, shown in Figure S2 (b), do not exhibit major variations with E_{det}.

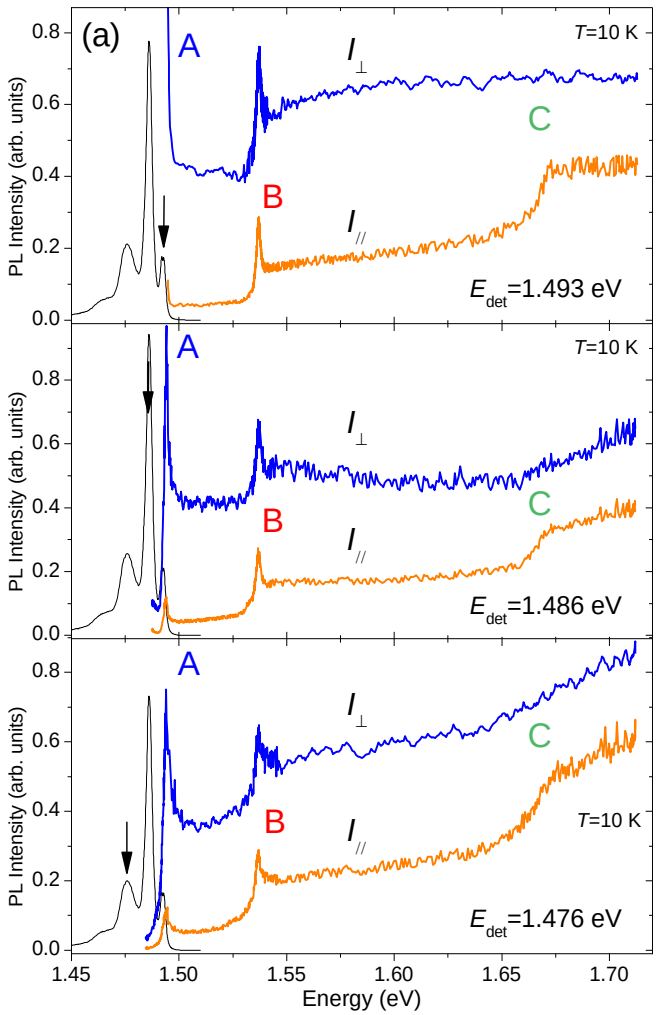

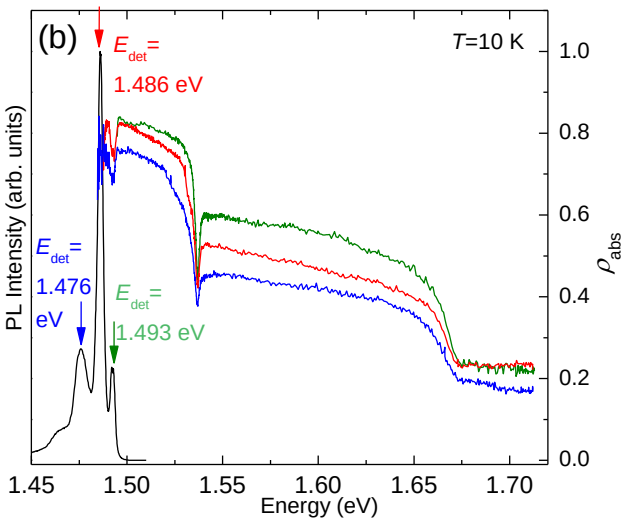

Figure S2. **(a)** PLE spectra recorded for different detection energies, E_{det}, and exciting photons with polarization vector orthogonal (intensity $I_\perp$) and parallel (intensity $I_{//}$) to the NW $\hat{c}$ axis. The arrows on the PL spectra, shown for reader's convenience, indicate the PLE detection energies. The intensity axis refers to PLE spectra, only. **(b)** Absorption polarization degree (right axis) obtained for different E_{det}'s, as indicated on the PL spectrum.

We notice that the A and B excitonic features (resonances in the PLE spectra and dips in the polarization degree, see main text) in both panels (a) and (b) become more prominent as E_{det} gets closer to the A exciton energy.

S3. Evaluation of the contribution of the continuum of states to transitions B and C.

$I_\perp / I_{//}$ is the ratio between the PLE intensity obtained with laser polarization vectors orthogonal ($I_\perp$) and parallel ($I_{//}$) to the NW $\hat{c}$ axis. In principle, this quantity permits to estimate the relative strength of the absorption intensity, which depends on the polarization of the absorbed photons. Figure S3 (a) shows the polarization-dependent PLE spectra displayed in Figure 4 (a) of the main text. Figure S3 (b) sketches the band structure of a WZ crystal. Transitions from the higher-energy valence bands (VBs) A, B, and C to the lowest conduction band (CB) both at $k = 0$ (Γ) and $k \neq 0$

are indicated. The sketch highlights the contribution of the continuum of states (*i.e.*, $k \neq 0$) of band A at the energy of the B resonance and beyond. Similarly, transition energies corresponding to the C resonance and its continuum are resonant with $k \neq 0$ transitions involving A and B VBs. In Figure S3 (a), the nearly horizontal dashed lines are used to approximately estimate the contributions to B and C resonances from the continuum of states of other bands. These estimated contributions are given by the numbers shown in the figure together with those relative to the total PLE intensities at each resonance.

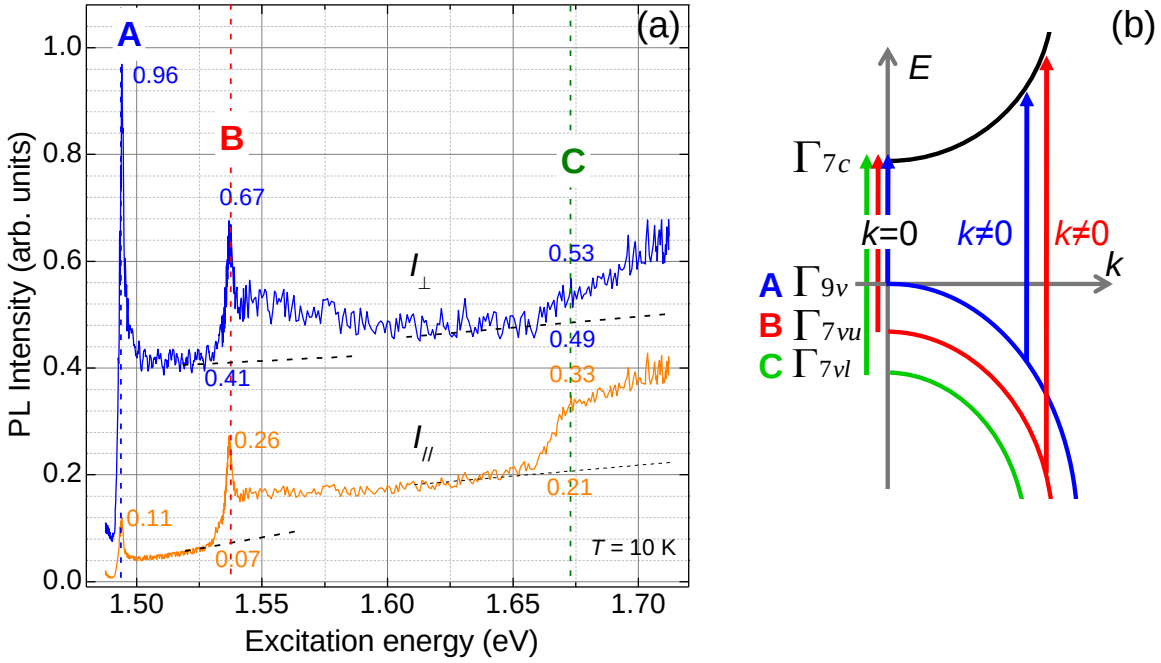

Figure S3. **(a)** PLE spectra recorded with laser polarization vector orthogonal ($I_\perp$) and parallel ($I_{//}$) to the $\hat{c}$ axis. The nearly horizontal lines are meant to estimate the background contribution to B and C resonances from continuum of states due to other VB states. These estimated contributions are given by the numbers shown in the figure together with those relative to the total PLE intensities at the A, B, and C resonances. **(b)** Simplified sketch of transitions from the three valence bands to the lowest conduction band of WZ. Conduction- and valence-band symmetries at Γ ($k = 0$) point and transition labels are indicated. Both transitions at Γ and at $k \neq 0$ are shown.

S4. Filtering the dielectric mismatch effect from PLE spectra.

The ratio $I_\perp / I_{//}$ between the PLE intensity obtained using a laser with polarization vector orthogonal ($I_\perp$) and parallel ($I_{//}$) to the NW $\hat{c}$ axis is significantly influenced by the dielectric

mismatch effect. The quantitative estimate of this effect by finite-difference time-domain (FDTD) calculations, $(I_{//}/I_{\perp})_{\text{calc}}$, is shown in Figure 4 (b) of the main text and in Figure S4 (a). By multiplying the measured $I_{\perp}$ PLE spectrum by the values of $(I_{//}/I_{\perp})_{\text{calc}}$ we essentially filter out the effect of the dielectric mismatch. The resulting PLE spectrum is shown in Figure S4 (b) by a dark blue line. Consequently, the corrected $I_{\perp}/I_{//}$ ratio changes from 9 to 40 for A, from 1.4 to 4 for B, and from 0.3 to 0.4 for C. In turn, this procedure allowed us to isolate and evaluate the strength of optical selection rules alone in WZ materials.

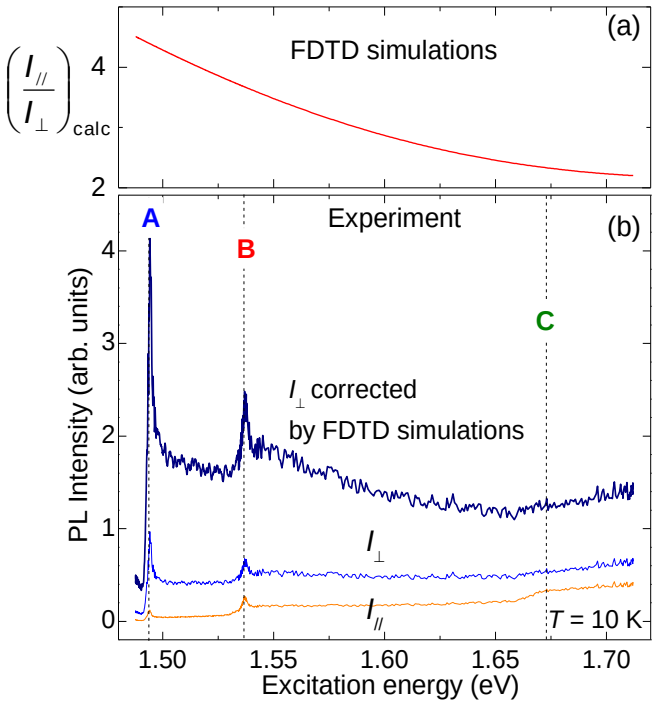

Figure S4. **(a)** The line shows the attenuation ratio $(I_{//}/I_{\perp})_{\text{calc}}$ due to the dielectric mismatch effect as found by finite difference time-domain simulations, FDTD. Those data are used to remove the dielectric mismatch effect from the $I_{\perp}$ PLE spectrum. **(b)** PLE spectra taken at T =10 K with detection energy set at 1.486 eV. The spectra were collected by exciting the sample with light polarization vector parallel (orange line) and perpendicular (blue lines) to the NW $\hat{c}$ axis. The dark-blue line gives the $I_{\perp}$ PLE spectrum multiplied by the $(I_{//}/I_{\perp})_{\text{caòc}}$ as calculated by the FDTD simulations shown in (a).

S5. Room temperature PLE spectra

We show the PLE spectra recorded at room temperature in order to demonstrate the persistence of the low temperature band structure features, namely, the A, B, and C absorption edges and their polarization.

Figures S5 (a) and (b) show the PLE spectra at T = 290 K of the ensemble of WZ InP NWs in backscattering and grazing incidence configuration, respectively. In the latter case two absorbed photon polarizations were considered: parallel (orange line) and perpendicular (blue line) to the NW $\hat{c}$ axis. The pink line shows the degree of linear polarization ρ_{abs} of absorbed light, as calculated by applying Eq. (1) of the main text to the two PLE spectra. As expected, no dips in ρ_{abs} at the A and B excitonic resonances are seen at 290 K, in agreement with the disappearance of the excitonic character of those transitions with increasing temperature.

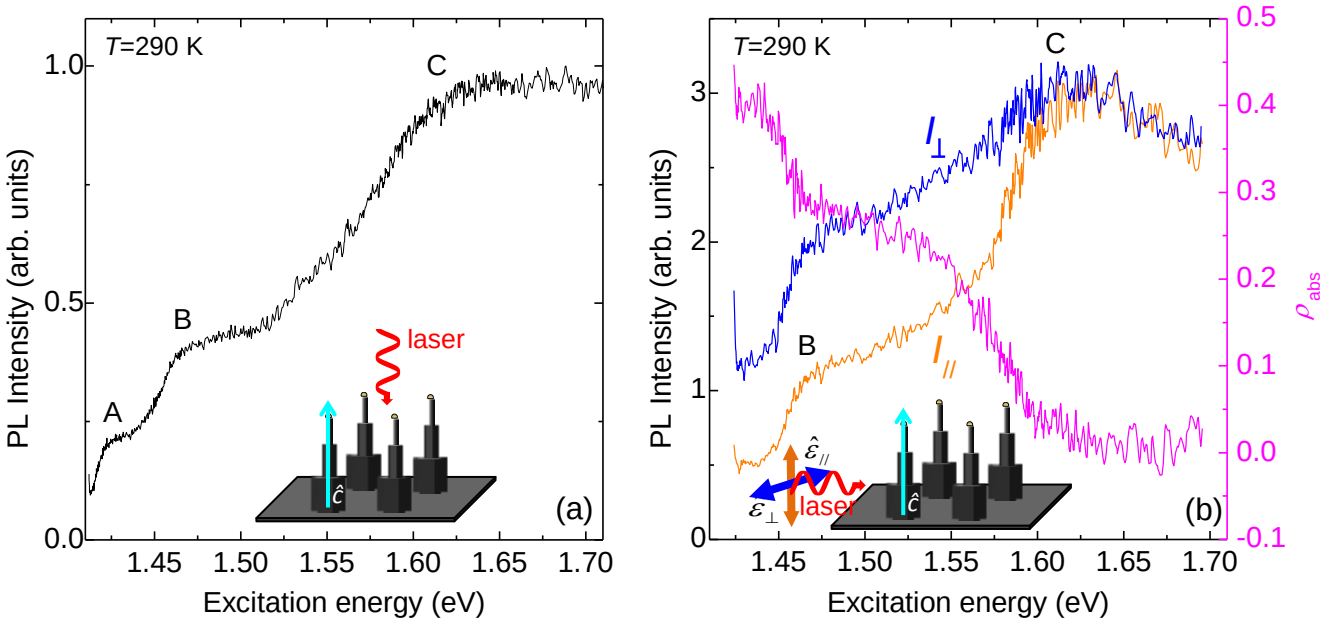

Figure S5 (a) PLE spectrum taken in a backscattering configuration (see sketch in the inset) at T=290 K with detection energy set at 1.409 eV. A, B, and C absorption edges are indicated. **(b)** PLE spectra taken at T=290 K with detection energy set at 1.422 eV. The spectra were excited with light polarization vectors parallel (orange line, $I_{//}$) and perpendicular (blue line, $I_{\perp}$) to the NW $\hat{c}$ axis (see sketch in the inset). The signals corresponding to the two light polarizations were recorded at each energy one just after the other. B and C absorption edges are indicated, while A is not observable because the detection energy is set right at the A energy. The pink line shows the degree of linear polarization ρ_{abs} of absorbed light, as calculated by applying Eq. (1) of the main text to the two PLE spectra.

Most importantly, the three-step feature of the absorption spectrum is maintained also at room temperature, especially in the backscattering configuration. PLE at grazing incidence at room temperature is instead more challenging and noisier spectra were obtained. Nevertheless, the resulting absorption polarization degree permits us to quantify ρ_{abs} as a function of the absorbed photon energy. ρ_{abs} varies from about 0.4 near the A transition, decreases to about 0.3 at the B transition, and finally approaches zero at and above the C transition. The quantitative estimate of the dielectric mismatch is obtained by the FDTD calculations shown in Figure S4 (a). By multiplying the measured PLE spectrum of $I_{\perp}$ by the values of $\left(I_{//}/I_{\perp}\right)_{calc}$ we can filter out the effect of the dielectric mismatch. After subtraction of the contributions from continuum states to B and C transitions, we find $I_{\perp}/I_{//}$ ~ 13 for A, ~ 5 for B, and ~ 0.5 for C. These values allow us to conclude that the selection rules (and the ensuing results on the strength of the spin-orbit coupling) summarized in the table in Figure 4 (b) of the main text still hold at room temperature.

S6. Lorenz model of the optical dispersion by excitons

In a simple picture of optical media, the presence of energy-dependent absorption and dispersion is described by a Lorentz oscillator model resulting in a frequency-dependent complex permittivity $\tilde{\varepsilon}$, whose real ε_1 and imaginary ε_2 parts are given by:

$$\varepsilon_1 = 1 + L\frac{\omega_0^2 - \omega^2}{\left(\omega_0^2 - \omega^2\right)^2 + \gamma^2\omega^2} \quad \text{and} \quad \varepsilon_2 = L\frac{\gamma\omega}{\left(\omega_0^2 - \omega^2\right)^2 + \gamma^2\omega^2}.$$

L is a constant dependent on medium's carrier mass and atomic density, ω_0 is the Lorentz oscillator resonance frequency, and γ takes into account dissipation phenomena resulting in a broadening of the frequency-dependent optical constants.

In the restricted energy range close to the A exciton resonance in the PLE spectra shown in Figures 4 (a) and 5 (b), we take the Lorentz oscillator as an effective means to model absorption and dispersion. In the Lorentz model for the exciton we fixed the energy of the A exciton absorption-

peak ($\hbar\omega_0 = 1.494$ eV) and its line-width ($\gamma \sim 2$ meV) as derived by the experimental data. Unfortunately, measurements or calculations of the permittivity of WZ InP that take into account excitonic effects at the band-gap have not been reported in the literature. Therefore, the *L* constant value in the above equations was treated as a parameter to better reproduce the absorption polarization degrees shown in Figure 6 (c) of the main text. Likewise, β in Equation (3) of the main text (measuring the ratio between $I_{\perp}$ and $I_{//}$ due to WZ selection rules) was set equal to 280.

---

[1] Alouane, M. H. H.; Chauvin, N.; Khmissi, H.; Naji, K.; Ilahi, B.; Maaref, H.; Patriarche, G.; Gendry, M.; C Bru-Chevallier, C. *Nanotechnology* **2013** *24*, 035704.

[2] Bao, J.; Bell, D. C.; Capasso, F.; Wagner, J. B.; Mårthensson, T.; Trägårdh, J.; Samuelson, L. *Nano Lett.* **2008**, *8*, 836-841.

[3] Gao, Q.; Saxena, D.; Wang, F.; Fu, L.; Mokkapati, S.; Guo, Y.; Li, L.; Wong-Leung, J.; Caroff, P.; Tan, H. H.; Jagadish, C. *Nano Lett*. **2014** *14*, 5206-5211.

[4] Vu, T. T. T.; Zehender, T.; Verheijen, M. A.; Plissard, S. R.; Immink, G. W. G.; Haverkort, J. E. M.; Bakkers, E. P. A. M. *Nanotechnology* **2013** *24*, 115705 1-6.

[5] De Luca, M.; Polimeni, A.; Fonseka, H. A.,; Meaney, A. J.; Christianen, P. C. M.; Maan, J. C.; Paiman, S.; Tan, H. H.; Jagadish, C.; Capizzi, M. *Nano Lett.* **2014**, *14*, 4250-4256.